reflect local perturbations in melt delivery. These may be short-lived phenomena, relative to the convective process that supports the long-wavelength pattern. The variation in size, location and longevity of magmatic segments suggests that oceanic crust may be a patchwork (in plan view) of lozenge-shaped igneous units which are each associated with a distinctive set of physical and chemical characteristics in three dimensions, and whose size is determined by the scale of the parent magmatic segment.

We thank the US ONR and NSF for supporting this work, the captain, crew, students and technical groups (SeaMARC II and Sea Beam) at sea, Dr R. Tyce for his programming contribution, Antoinette Padgett for preparing the manuscript and illustrations, and Drs M. McNutt and N. Sleep for constructive reviews.

1. Wilson, J. T. *Nature* **207**, 343-347 (1965).
2. Coode, A. M. *Can. J. Earth Sci.* **2**, 400-401 (1965).
3. Davis, E. E., Currie, R. G., Sawyer, B. S. & Kosalos, J. G. *Mar. Technol. Soc. J.* **20**, 17-27 (1986).
4. Tyce, R. C. *Mar. Technol. Soc. J.* **20**, 4-16 (1986).
5. Macdonald, K. C. & Fox, P. J. *Nature* **302**, 55-57 (1983).
6. Macdonald, K. C., Sempere, J.-C. & Fox, P. J. *J. geophys. Res.* **89**, 6049-6069 (1984); **91**, 1050-10510 (1986).
7. Lonsdale, P. *J. geophys. Res.* **88**, 9393-9406 (1983); *Geol. Soc. Am. Bull.* **96**, 313-327 (1985).
8. Hey, R. N., Kleinrock, M. C., Phipps Morgan, J. M., Atwater, T. M. & Searle, R. C. *J. geophys. Res.* **91**, 3369-3394 (1986).
9. Schouten, H., Klitgord, K. D. & Whitehead, J. A. *Nature* **317**, 225-229 (1985).
10. Crane, K. *Earth planet. Sci. Lett.* **72**, 405-414 (1985).
11. Klitgord, K. & Mammerickx, J. *J. geophys. Res.* **87**, 6725-6750 (1982).
12. Kastens, K. A., Ryan, W. B. F. & Fox, P. J. *J. geophys. Res.* **91**, 3469-3488 (1986).
13. Gallo, D. H., Fox, P. J. & Macdonald, K. C. *J. geophys. Res.* **91**, 3455-3468 (1986).
14. Langmuir, C. H., Bender, J. F. & Batiza, R. *Nature* **322**, 422-429 (1986).
15. Klein, E. M. *et al.* (abstr.) *Eos* **68**, 1540 (1987).
16. Detrick, R. S. *et al. Nature* **326**, 35-41 (1987).
17. Macdonald, K. C. & Fox, P. J. *Earth planet. Sci. Lett.* **88**, 119-131 (1988).
18. Thompson, G., Bryan, W. B., Ballard, R., Hamuro, K. & Melson, W. G. *Nature* **318**, 429-433 (1985).
19. Thompson, G., Bryan, W. B. & Humphris, S. E. *Geol. Soc. Lond. spec. Publ.* (in the press).
20. Schouten, H. & Klitgord, K. D. *Earth planet. Sci. Lett.* **59**, 255-266 (1982).
21. Whitehead, J. A., Dick, H. J. B. & Schouten, H. *Nature* **312**, 146-147 (1984).
22. Elthon, D., Casey, J. F. & Komor, S. *J. geophys. Res.* **87**, 8717-8734 (1982).
23. Madsen, J. A., Forsyth, D. W. & Detrick, R. S. *J. geophys. Res.* **89**, 9997-10016 (1984).
24. Sinton, J. M., Wilson, D. S., Christie, D. M., Hey, R. N. & Delaney, J. R. *Earth planet. Sci. Lett.* **62**, 193-207 (1983).
25. Batiza, R. & Margolis, S. H. *Nature* **320**, 439-441 (1986).
26. Oldenburg, C. M., Spera, F. J. & Yuen, D. A. *J. geophys. Res.* (submitted).
27. Blackinton, J. G., Hussong, D. M. & Kosalos, J. *Proc. offshore Technol. Conf.* **4478**, 307-311 (1983).
28. Macdonald, K. C., Sempere, J.-C., Fox, P. J. & Tyce, R. *Geology* **15**, 993-997 (1987).
29. Pollard, D. D. & Aydin, A. *J. geophys. Res.* **89**, 10017-10028 (1984).
30. Johnson, H. P. *et al. J. geophys. Res.* **88**, 2297-2315 (1983).
31. Macdonald, K. C., Haymon, R. M., Miller, S. P., Sempere, J.-C. & Fox, P. J. *J. geophys. Res.* **93**, 2875-2898 (1988).
32. Phipps Morgan, J. M. & Parmentier, E. M. *J. geophys. Res.* **90**, 8603-8612 (1985).
33. Sempere, J.-C. & Macdonald, K. C. *Tectonics* **5**, 151-163 (1986).
34. Schouten, H., Dick, H. J. B. & Klitgord, K. D. *Nature* **326**, 835-839 (1987).
35. Mammerickx, J. *J. geophys. Res.* **89**, 1817-1828 (1984).
36. Madsen, J. A., Fox, P. J. & Macdonald, K. C. *J. geophys. Res.* **91**, 3439-3454 (1986).
37. Bender, J. F., Langmuir, C. H., Kastens, K. & Ryan, W. (abstr.) *Eos* **69**, 488 (1988).
38. Forsyth, D. W. & Wilson, B. *Earth planet. Sci. Lett.* **70**, 355-362 (1984).
39. Pollitz, F. F. *Nature* **320**, 738-741 (1986).

ARTICLES

Laser-driven implosion of thermonuclear fuel to 20 to 40 g cm^{-3}

R. L. McCrory, J. M. Soures, C. P. Verdon, F. J. Marshall, S. A. Letzring, S. Skupsky, T. J. Kessler, R. L. Kremens, J. P. Knauer, H. Kim, J. Delettrez, R. L. Keck & D. K. Bradley

Laboratory for Laser Energetics, University of Rochester, 250 East River Road, Rochester, New York 14623-1299, USA

Inertial fusion requires the compression of fusion fuel to densities approaching 1,000 times the density of liquid DT. Compression of DT to densities in the range of 100 to 200 times its liquid density has been achieved using cryogenically cooled solid-fuel-layer DT-filled capsules irradiated directly with high-intensity symmetric short-wavelength laser radiation.

THE compression of deuterium-tritium (DT) to high densities represents a critical test of the feasibility of laser fusion[1]. An extremely high degree of drive uniformity and symmetry and an ablative low-entropy implosion of fuel capsules are prerequisites for high-density compression. One approach to inertial fusion currently being investigated involves the conversion of laser energy to X rays to drive the implosion (indirect or *hohlraum* drive)[2]. The alternative approach, direct laser irradiation of capsules, may be more energy-efficient than indirect drive if stringent drive uniformity requirements are achieved[3]. A critical test of the potential of direct drive to meet these requirements has been carried out in cryogenic target experiments conducted on the OMEGA laser facility at the University of Rochester. These experiments, which use a comprehensive set of diagnostics to characterize the time history of the implosion and the compressed-fuel conditions, have resulted in the first direct measurement of high fusion-fuel areal density produced by laser fusion. Compressed DT fuel densities of ~20-40 g cm^{-3}, 100 to 200 times the density of liquid DT (100-200 × LD), were achieved, the highest yet attained in direct-drive inertial fusion experiments.

Two sets of implosion experiments were carried out. The first set, in which the fuel was initially in the gas phase, was conducted to develop, activate and calibrate diagnostics needed to characterize the acceleration phase of the target implosion and to measure the core conditions at the time of neutron production. These experiments produced fuel densities greater than 50 × LD; the results were used for a detailed comparison of theoretical calculations. Details of this series of experiments have been reported previously[4]. For the series of target implosion experiments described here the fuel was initially in the solid phase. Cryogenic cooling was required, together with substantial improvements to both target irradiation and diagnostic techniques, to achieve and measure greatly increased compressed, fuel densities of ~100-200 × LD.

Previous experiments[5] have reported compressed-fuel densities of ~100 × LD using nuclear activation techniques that measure the shell areal density ($\rho\Delta R$) of the material surrounding the thermonuclear fuel. The compressed-fuel density was deduced by assuming mass conservation, a one-dimensional model of the compressed core and pressure balance, to relate the shell areal density to that of the fuel. In the experiments reported here the fuel areal density (ρR) is measured directly during the time of neutron production. This measurement is insensitive to the shell areal density and to the temperature of the imploded material and is independent of the amount of shell

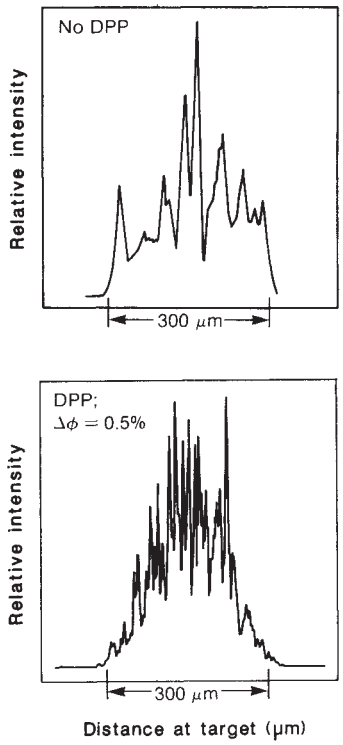

Fig. 1 Line-outs of the target-plane intensity distributions show marked improvement in uniformity (for low-frequency modes) after phase conversion. Numerous hot spots, each about 5% to 10% of the target-plane beam diameter, are replaced by a reproducible intensity envelope that contains small-scale speckle.

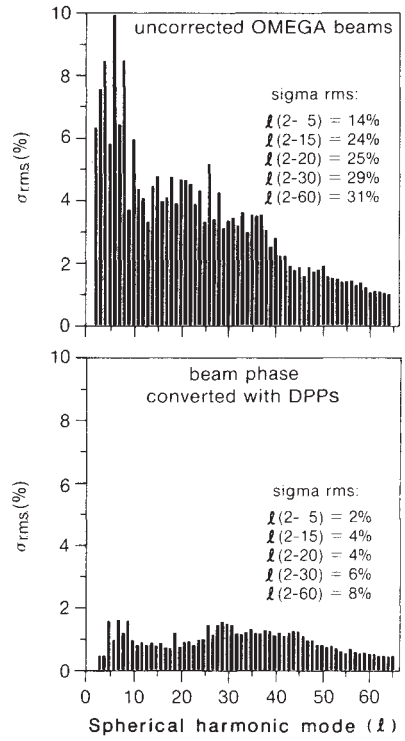

Fig. 2 Overall improvement in the irradiation uniformity on target is assessed by computing a 24-beam superposition of intensities and a spherical harmonic decomposition. The intensity nonuniformity ($\sigma_{r.m.s.}$%) is reduced by a factor of 6 for modes $l=2$ to 20, and by a factor of 4 for modes $l=2$ to 60. Smoothing by 1% of the beam diameter is assumed.

material mixed within the fuel region; it is the first such measurement of highly compressed thermonuclear fuel.

Experimental configuration

The OMEGA laser is a 24-beam Nd:phosphate-glass laser that is frequency-tripled to operate in the ultraviolet (351 nm) using the polarization mismatch scheme[6]. Experiments were performed by irradiating targets with 1,000- to 1,500-J ultraviolet radiation delivered in 600 to 700-ps (FWHM) gaussian-shaped laser pulses. Before these experiments major improvements were made to the OMEGA laser system irradiation-uniformity on target. These improvements were implemented as a result of comprehensive measurements of both beam amplitude and phase, in conjunction with numerical models to simulate sources of target-plane irradiation nonuniformity. Phase defects throughout the amplifier chain, the KDP conversion cells and transport optics were identified as dominant factors controlling the intensity profile in the target plane.

Hot-spot intensity nonuniformities in the OMEGA target plane were found to be caused principally by spatial variations in the near-field phase front of each laser beam. In order to increase the uniformity of target irradiation we implemented, through the use of two-level distributed phase plates (DPPs)[8], a technique originally suggested by Kato *et al.*[7] that modifies the phase fronts of the laser beams to produce ~250,000 overlapping 'beamlets' on target. (A DPP is composed of an ordered array of transparent hexagonal elements in which phase retardation is randomly distributed among the elements by using a thin-film layer to introduce optical path differences.) Figure 1 shows cross sections of the target-plane intensity distributions before and after phase conversion with a DPP; the numerous hot spots are replaced by a reproducible and uniform envelope that contains small-scale speckle.

The overall target irradiation uniformity is computed by superposing the intensities from all 24 beams of the OMEGA system. The resulting intensity pattern can be then decomposed into spherical harmonics. Figure 2 shows the computed overall improvement of the target irradiation uniformity through the use of the DPPs. The intensity nonuniformity, $\sigma_{r.m.s.}$(%), is improved by a factor of 6 for low-order modes ($2 \leq l \leq 20$) and by a factor of 4 for modes 2 to 60. Smoothing in the plasma by 1% of the beam diameter (~3 μm) is assumed. Beam-to-beam energy balance was ~5%, beam-to-beam timing error was ≤3 ps and the individual beam placement on target was accurate to ≤10 μm. Based on the above measured quantities and the calculated superposition, the illumination nonuniformity for the entire series of experiments was estimated to be ≤12% ($\sigma_{r.m.s.}$).

An integrated cryogenic system, which used the fast-refreeze technique originally developed by KMS Fusion, Inc. (Ann Arbor, Michigan, USA)[9], was used in the experiments for producing, positioning, protecting and documenting glass shells containing a frozen DT layer. The target-positioning and viewing system allows for three-dimensional positioning of the cryogenically cooled target to within ±5 μm and measurement of the frozen-fuel-layer thickness and uniformity to within ±1 μm. The targets were glass shells with a diameter of 200 to 300 μm, wall thickness of 3 to 7 μm. These were filled with DT at 100 atm and which forms a layer ~5 μm thick next to the glass shell when cooled below 19 K. The targets were held at the center of the OMEGA target chamber by spider-silk fibres (<0.5 μm in diameter) drawn across a U-shaped mount. To ensure mechanical stability the target and fibre assembly was coated with a 0.2-μm-thick layer of parylene. The mounted target was cooled to below the freezing temperature of DT in a liquid-He-cooled shroud. The frozen DT layer was prepared further by repeated heating with an Ar-ion laser followed by rapid cooling,

until a layer with a thickness variation of less than 20% was obtained. Approximately 40 ms before target irradiation, the cooling shroud was rapidly retracted, exposing the target to the ambient environment for ~10 ms. (The length of time required for the DT layer to melt was ~30 ms.)

A number of complementary nuclear, X-ray and particle diagnostic systems, including a four-frame high-speed X-ray framing camera and polycarbonate (CR-39) nuclear track detectors, were used to measure simultaneously the target performance[4].

Experimental results

Measurements of the absorption and the fractional conversion of the absorbed energy into X rays were found to be in good agreement with one-dimensional hydrodynamic code simulations of targets used in these experiments. Typically 60% to 80% of the incident laser energy was absorbed by the target[4]. Measurements of the X-ray conversion efficiency show that approximately 15% to 20% of the absorbed energy was converted to X rays with energies below 9 keV (ref. 4). Time- and space-resolved measurements of the X-ray emission were used to measure the time history of the implosion. The results of these measurements are in general agreement with the one-dimensional code predictions, implying that the actual target drive (the fraction of the absorbed energy converted to kinetic energy of the pusher) is close to that predicted by the simulations. Figure 3 shows the result of a series of X-ray pinhole photographs obtained on a single shot with a four-frame X-ray framing camera[10]. Analysis of these data and comparison to the code prediction are shown in Fig. 4. The good agreement between the observed and predicted shell radius as a function of time confirms the accuracy of the theoretical modelling of the fractional incident laser energy converted into shell kinetic energy.

The fuel condition at the time of neutron production was measured with the 'knock-on' diagnostic[11]. In this technique, the number of deuterium and tritium ions scattered by 14.1-MeV fusion neutrons is detected using a series of polycarbonate (CR-39) track-detector foils[11]. The number of such ions (knock-ons) is directly proportional to the fuel ρR. Three sets of knock-on detectors were positioned at nearly mutually orthogonal positions about the target, both to increase collecting solid angle and to provide a representative sample of the average knock-on flux. The diameter and length of tracks in the CR-39 foils were

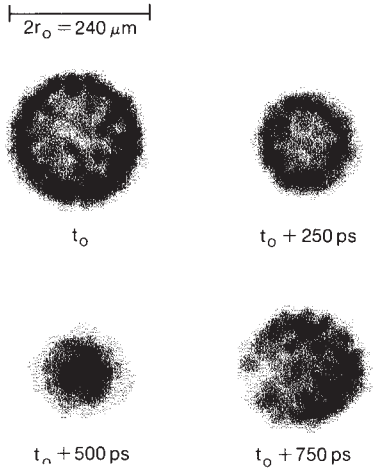

Fig. 3 A set of X-ray images taken on a cryogenic target experiment (number 16054) with the four-frame gated intensifier system coupled to an X-ray pinhole camera. The temporal separation between frames is 250 ps and the frame width is 125 ps. For reference, the first image is taken as zero time (t_0). These images have not been corrected for spatial nonuniformity in the gain of the intensifier.

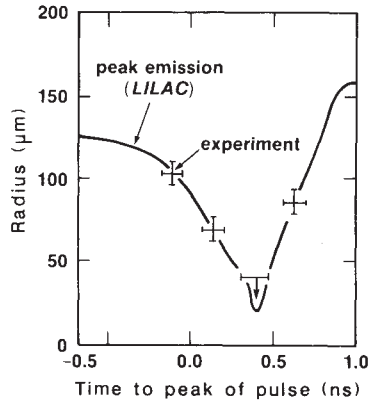

Fig. 4 Measured shell X-ray emission radius versus time determined from the framing camera images in Fig. 3 and one-dimensional (LILAC) code predictions of the same.

used to separate the knock-ons from background protons. This method of background discrimination was tested on low ρR implosions for which there should not be any significant slowing down of the knock-ons in the target; the expected knock-on spectrum is well known from the n-D and n-T elastic-scattering cross sections[12]. The measured results were in good agreement with the spectrum predicted theoretically[11].

The track selection criteria limit the number of knock-ons detected by a single foil to a discrete energy window that includes only a fraction of the knock-on spectrum. This fraction depends on the distortion of the knock-on spectrum caused by energy loss of the particles as they pass through the target. In general, the knock-on energy loss is a function of ρR, $\rho\Delta R$ and temperature. We used a multi-foil configuration that detects a nearly constant fraction of the knock-on flux, independent of ρR, $\rho\Delta R$ and temperature. Figure 5 shows calculated knock-on spectra for both low ρR_{total} and high ρR_{total} using a five-foil configuration. The deuterons have a longer range than the tritons and therefore can penetrate a higher value of total areal density ($\rho R_{\text{total}} = \rho R + \rho\Delta R$). For the low-density case ($\rho R_{\text{total}} = 20\ \text{mg cm}^{-2}$) the peak of the deuteron spectrum (produced from near head-on collisions between deuterons and neutrons) lies in the window of foil 5, whereas for the high-density case ($\rho R_{\text{total}} = 40\ \text{mg cm}^{-2}$) the deuteron peak has shifted to foil 3. Although the fraction of deuterons detected in any one of foils 2 to 5 differs depending on the degree of slowing down in the target, the sum of knock-ons detected in foils 2 to 5 is a nearly constant fraction, f_D, of the total knock-on number. The fraction is $f_D = 0.085$, to within ±5%, for $\rho R_{\text{total}} \leq 50\ \text{mg cm}^{-2}$. This is an upper bound on f_D and is independent of the amount of slowing down. For higher ρR_{total}, f_D will always be less than 0.085 as the deuterons are slowed down out of the windows of the foils. The fuel areal density can be obtained from the number of detected deuteron knock-on tracks by

$$\rho R = 5.4 \times 10^3 \frac{K_D}{Y_N}\left(\frac{4\pi}{\Delta\Omega}\right)\frac{1}{f_D}$$

where K_D is the sum of knock-on tracks detected in foils 2 to 5, $\Delta\Omega$ is the solid angle subtended by the foils and Y_N is the neutron yield. As f_D appears in the denominator of this expression, by using its upper bound we are able to obtain a lower bound for ρR.

The fuel density averaged over the time of thermonuclear burn (neutron-averaged density) can be estimated from the measured ρR by assuming a simple model for the distribution of the fuel in the burn region. One such model (the 'ice-block' model) assumes that the fuel is compressed uniformly into a region of radius R and that neutron production occurs at the

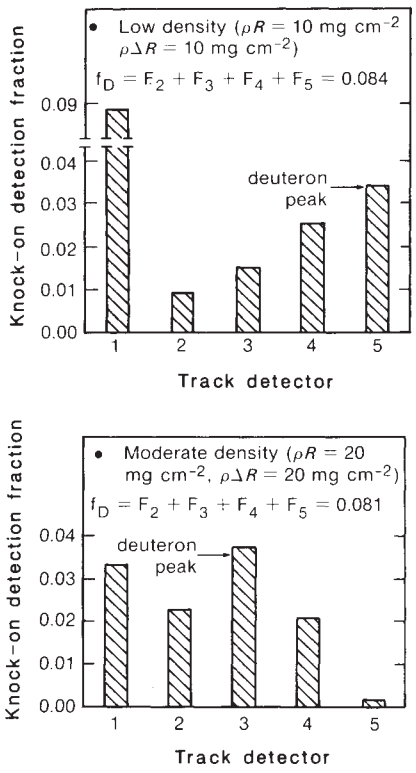

Fig. 5 Relative number of knock-ons in each of the five CR-39 foils for $\rho R_{total} = 20$ mg cm^{-2} and $\rho R_{total} = 40$ mg cm^{-2}. Each foil is preceded by different amounts of moderating material to bring different parts of the knock-on spectrum into the foil's energy window. For deuterons (D) and tritons (T) the knock-on-energy range (MeV) detected by each foil is: (1) D (6.2-7.6), T (7.3-10.6); (2) D (8.2-9.7), T (9.8-10.6); (3) D(9.4-10.7); (4) D (9.8-11.1); (5) D (11.0-12.6). For $\rho R \gtrsim 5$ mg cm^{-2} all tritons will have slowed down below ~9.8 MeV so that only deuterons will produce tracks in the energy window for foils 2 to 5.

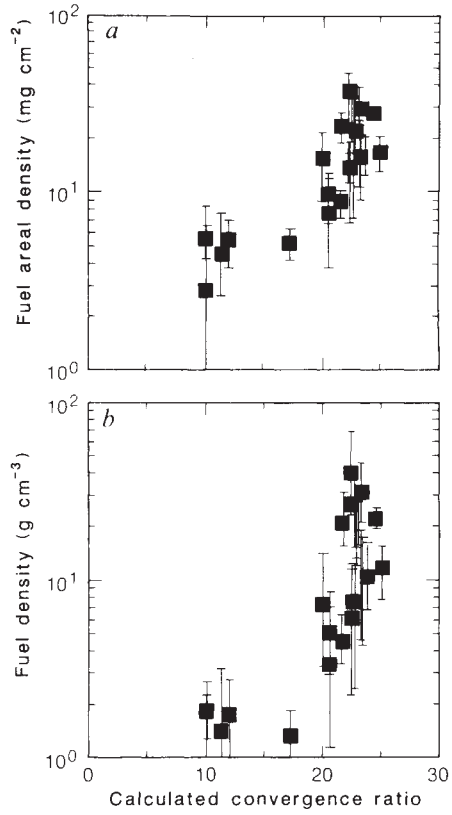

Fig. 6 *a*, Measured fuel areal density plotted as a function of calculated convergence ratio (C_R) for cryogenic target experiments (the convergence ratio is defined as initial fuel-pusher interface radius divided by the minimum fuel-pusher interface radius). *b*, Fuel density inferred from measured fuel areal density plotted as a function of C_R assuming the ice-block model[13] for the fuel and neutron burn distribution.

centre of this region[13]. Under the assumption that all of the initial mass of fuel, M, is compressed into this region, the fuel density is $\rho = (4\pi/3M)^{1/2}(\rho R)^{3/2}$. If any of the assumptions of the model are relaxed, a higher estimate of fuel density would result. For example, if the neutron production were constant across the fuel volume the resulting inferred density would be approximately 50% higher than would be estimated on the basis of the ice-block model. Numerical models of the implosion always suggest a higher fuel density at the edge of the core due to a near pressure-balance at the time of stagnation. This effect will always produce higher average densities for the same ρR than those predicted by the ice-block model.

Measurements of the neutron-averaged fuel areal density were made on a series of cryogenic target experiments. The measured fuel areal densities (obtained from the knock-on diagnostic) and the fuel mass densities inferred using the ice-block model are shown in Fig. 6. The error bars are calculated from the combined relative errors in measurement of the neutron yield and the knock-on flux. The highest values of fuel ρR ~20-35 mg cm^{-2}. The corresponding fuel densities inferred from these experimental results are ~20-40 g cm^{-3}.

The observed neutron yields (10^6-10^8) and neutron-weighted fuel areal densities (20-35 mg cm^{-2}) were below those predicted by one-dimensional simulations. The yields were ~10^{-3} of predicted values whereas the fuel areal densities were typically 0.2 to 0.5 of the predicted values. The reasons for these discrepancies are still being investigated, but we suggest that departures from one-dimensional performance are due primarily to residual imperfections in the level of illumination uniformity presently attained with the OMEGA system.

Summary

A series of direct-illumination, ablatively driven implosion experiments was carried out on the 24-beam 351-nm OMEGA laser system using frozen-fuel DT-filled glass shell targets. Distributed phase plates were used to improve the irradiation uniformity levels on target. Measurements of the energy coupling to the target confirm the high level of collisional absorption and efficient conversion of the absorbed energy to pusher kinetic energy expected with short-wavelength laser illumination. Typical measured absorption fractions were ~60%-80% of the incident laser energy and are in good agreement with predicted values. Likewise, the measured and predicted shell radius-versus-time were in good agreement with one-dimensional simulations. These results show that gross features of the implosion phase are modelled accurately by one-dimensional simulations.

Using track detectors to measure the elastically scattered fuel ions, fuel areal densities of ~20-35 mg cm^{-2} were measured directly, implying neutron-averaged fuel densities of ~20-40 g cm^{-3} (100-200 × LD). These are the first direct measurements of the fuel areal density of highly compressed fusion fuel that do not involve any assumptions about temperature or fuel-shell mixing. The inferred fuel densities are the highest attained for any direct-drive laser-fusion experiment.

This work was supported by the United States Department of Energy Division of Inertial Fusion and by the Laser Fusion

Feasibility Project at the Laboratory for Laser Energetics, which has the following sponsors: Empire State Electric Energy Research Corporation, New York State Energy Research and Development Authority, Ontario Hydro, and the University of Rochester. Such support does not imply endorsement of the content by any of the above parties.

Received 27 May; accepted 15 July 1988.

1. Nuckolls, J., Wood, L., Thiessen, A. & Zimmerman, G. *Nature* **239**, 139-142 (1972).
2. Nuckolls, J. *Physics Today* **35**, 24-31 (1982).
3. Craxton, R. S., McCrory, R. L. & Soures, J. M. *Sci. Am.* **255**, 68-79 (1986).
4. McCrory, R. L. *et al. Proceedings of SPIE* Vol. 913 (1988); *Laboratory for Laser Energetics Annual Report 1987*, DOE/DP 40200-64, 93-106 (1988).
5. *Laser Program Annual Report—1984*, Lawrence Livermore National Laboratory, Livermore, California, UCRL-50021-84, 5-35-5-38 (1985).
6. Craxton, R. S. *Opt. Commun.* **34**, 474-479 (1980); Seka, W., Jacobs, S. D., Rizzo, J. E., Boni, R. & Craxton, R. S. *Opt. Commun.* **34**, 469-473 (1980).
7. Kato, Y. *et al. Phys. Rev. Lett.* **53**, 1057-1060 (1984).
8. *LLE Review* Vol. 33, Laboratory for Laser Energetics Quarterly Report, DOE/DP 40200-65, 1-10 (1987).
9. Musinski, D. L., Henderson, T. M., Simms, R. J. & Pattinson, T. R. *J. appl. Phys.* **51**, 1394-1402 (1980).
10. Kilkenny, J. D. *et al. Rev. sci. Instrum* (in the press).
11. Kacenjar, S., Goldman, L. M., Entenberg, A. & Skupsky, S. *J. appl. Phys.* **56**, 2027-2032 (1984); Skupsky, S. & Kacenjar, S. *J. appl. Phys.* **52**, 2608-2613 (1981).
12. *ENDF/D-IV Library*, National Neutron Cross Section Center, Brookhaven National Laboratory.
13. Campbell, E. M., Ploeger, W. M., Lee, P. H. & Lane, S. M. *Appl. Phys. Lett.* **36**, 965-967 (1980).

Thymic major histocompatibility complex antigens and the $\alpha\beta$ T-cell receptor determine the CD4/CD8 phenotype of T cells

Hung Sia Teh*‡, Pawel Kisielow*‡, Bernadette Scott*, Hiroyuki Kishi*, Yasushi Uematsu*, Horst Blüthmann† & Harald von Boehmer*

* Basel Institute for Immunology, 487 Grenzacherstrasse, CH-4058 Basel, Switzerland
† Central Research Units, F. Hoffmann-LaRoche, CH-4002 Basel, Switzerland

T-cell receptors and T-cell subsets were analysed in T-cell receptor transgenic mice expressing α and β T-cell receptor genes isolated from a male-specific, H-2D^b-restricted CD4$^-$8$^+$ T-cell clone. The results indicate that the specific interaction of the T-cell receptor on immature thymocytes with thymic major histocompatibility complex antigens determines the differentiation of CD4$^+$8$^+$ thymocytes into either CD4$^+$8$^-$ or CD4$^-$8$^+$ mature T cells.

THYMUS-derived lymphocytes (T cells) recognize antigen on the surface of antigen-presenting cells in the context of class I or class II major histocompatibility complex (MHC) molecules using the heterodimeric $\alpha\beta$ T-cell receptor (TCR)[1,2]. CD4 and CD8 molecules, expressed on the surface of T cells, bind to nonpolymorphic portions of class II and class I MHC molecules, respectively, and enhance the binding of the TCR to its ligand[3,4]. This binding of CD4 and CD8 molecules to MHC antigens may, in addition, contribute to signals leading to T-cell activation.

It is thought that the selection of the antigen-specific T-cell repertoire involves the negative selection (suppression or deletion) of autospecific T cells[5-8]. Some authors have also proposed that T cells are positively selected by thymic MHC antigens such that T cells, emerging from the thymus, bind foreign antigens predominantly in the context of self-MHC molecules[9-12]. To examine both aspects of T-cell repertoire selection we constructed TCR transgenic mice which expressed, on a large fraction of their T cells, a receptor which binds to H-Y antigen in the context of class I H-2D^b molecules. We used monoclonal antibodies that identify the transgenic receptor expressed in these mice to analyse negative selection in male $\alpha\beta$ transgenic H-2^b mice, which express the H-Y antigen as well as H-2D^b molecules. In addition, the analysis of female $\alpha\beta$ transgenic mice which express different thymic MHC antigens should reveal the possible impact of MHC molecules on the selection of T cells in the absence of nominal (H-Y) antigen.

In a previous report we have described our experiments on the mechanism of self-tolerance: from the comparison of $\alpha\beta$ transgenic male and female H-2^b mice we concluded that autospecific T cells were deleted in male mice. It was shown that this deletion involved predominantly immature CD4$^+$8$^+$ thymocytes, which contain the precursors of mature, single positive, CD4$^+$8$^-$ and CD4$^-$8$^+$ T cells[8,13].

There is less compelling evidence for the positive selection of T cells by thymic MHC antigens in the absence of nominal (H-Y) antigen: there have been reports of T cells recognizing foreign antigens predominantly in the context of those MHC molecules which they encountered during their maturation in the thymus[9-12]. It was also reported that animals that received large doses of class II MHC-antigen-specific antibodies were devoid of CD4$^+$8$^-$ T cells[14]. This could mean that antibodies can interfere with the positive selection of CD4$^+$8$^-$ T cells by thymic class II MHC antigens. These experiments do not, however, address the question of whether the $\alpha\beta$ TCR is involved in the selection process. On the basis of these and other experiments[15] one of us proposed that the interaction of the TCR on immature thymocytes with thymic MHC antigens will rescue immature T cells from programmed cell death and determine their further differentiation into mature CD4$^+$8$^-$ and CD4$^-$8$^+$ T cells. In the absence of nominal antigen, the interaction of the TCR with class II or class I thymic MHC antigens will direct the differentiation of immature T cells into CD4$^+$8$^-$ and CD4$^-$8$^+$ mature T cells, respectively[16,17]. This model predicts that in $\alpha\beta$ transgenic H-2^b mice the transgenic $\alpha\beta$ TCR should be expressed only on CD4$^-$8$^+$ and not CD4$^+$8$^-$ T cells because it was originally expressed on a class I-restricted CD4$^-$8$^+$ T cell which presumably was selected by class I MHC antigens in the thymus of C57B1/6 mice. Here we describe several observations, made in female $\alpha\beta$ transgenic mice, that are consistent with this model.

Firstly, the proportion of CD4$^-$8$^+$ thymocytes was elevated in $\alpha\beta$ transgenic H-2^b but not H-2^k or H-2^d mice. Secondly, using monoclonal antibodies specific for the transgenic receptor,

‡ Permanent addresses: Department of Microbiology, University of British Columbia, Vancouver, Canada V6T 1W5 (H.S.T.) and Institute of Immunology and Experimental Therapy, Polish Academy of Sciences, Wroclaw, Poland (P.K.).